Supporting Information

Single-atom Cu Anchored on Mo_2C Boosts Nitrite Electroreduction to Ammonia

Guohui Wang [1], Ruiyuan Ma [2], Nana Zhang[1], Yali Guo[1], Ke Chu[1]*

[1]*School of Materials Science and Engineering, Lanzhou Jiaotong University, Lanzhou 730070, China*

[2]*School of Architecture and Urban Planning, Lanzhou Jiaotong University, Lanzhou 730070, China*

17 January 2024

Note added after first publication: This Supplementary Information file replaces that originally published on 01 November 2023. An incorrect SEM image was originally included in Fig. S14(b) in error. The correct image has been included in this updated version. The discussion and conclusions of the paper are not affected.

Experimental Section

Materials

Na_2SO_4 (≥99.0%), $NaNO_2$ (≥99.0%), $C_5FeN_6Na_2O$ (≥99.0%), NH_4Cl (≥99.5%), N_2H_4 (≥99.0%), $C_7H_5NaO_3$ (≥99%), NaClO (5%), $C_6H_5O_7Na_3$ (≥98%), NaOH (≥96%), $(NH_4)_6Mo_7O_{24}$ (≥99.5%), $C_4H_6N_2$ (≥98%), $Zn(NO_3)_2·6H_2O$ (≥99.0%), $Cu(NO_3)_2·3H_2O$ (≥99.99%), H_2SO_4 (≥99.0%), H_2O_2 (≥99.0%), HCl (≥99.0%), C_2H_5OH (≥99.0%) and Nafion (5 wt.%) were provided from Sigma-Aldrich Chemical Reagent Co., Ltd. and Sinopharm Chemical Reagent Co., Ltd. Carbon cloth was purchased from Hengqiu Technology Co., Ltd. Ar (≥99.999%) was purchased from Lanzhou Xinwanke, Co., Ltd. All the reagents were analytical grade without further purification.

Synthesis of Mo_2C and Cu_1/Mo_2C nanosheets

Two solutions were prepared： solution 1 was prepared by dissolving 4 g $(NH_4)_6Mo_7O_{24}$ and 2.6 g $C_4H_6N_2$ in 80 ml of deionized water under stirring for 4 h, and solution 2 was prepared by dissolving 1.2 g $Zn(NO_3)_2·6H_2O$ in 40 ml of deionized water under stirring for 10 min. Then two solutions are mixed, stirred for 4 h to obtain a white precipitate. The obtained precipitates were collected by centrifugation, washed with deionized water and ethanol several times, and vacuum-dried at 80°C overnight. Afterwards, the white precipitates were transferred into a tube furnace and annealed at 850°C in a flowing Ar atmosphere for 1 h, obtaining Mo_2C. To prepare Cu_1/Mo_2C, an impregnation solution was prepared by dissolving 0.04 g $Cu(NO_3)_2·3H_2O$ in 50 mL deionized water. Mo_2C powder was then dipped into the impregnation solution for 2 h and then taken out and dried at 80 °C, obtaining Cu_1/Mo_2C.

Characterization

X-ray diffraction (XRD) pattern was recorded on a Rigaku D/max 2400 diffractometer. Scanning electron microscopy (SEM) was carried out on a ZEISS GeminiSEM-500 microscope. Transmission electron microscopy (TEM), high-resolution transmission electron microscopy (HRTEM) were carried out on a

Tecnai G^2 F20 microscope. Synchrotron radiation-based X-ray absorption spectroscopy (XAS) measurements were conducted at the BL14W1 beamline in Shanghai Synchrotron Radiation Facility (SSRF).

Electrochemical measurements

Electrochemical measurements were performed on a CHI-660E electrochemical workstation with a standard three-electrode system, where catalyst coated on carbon cloth (CC, 0.5 mg cm^{-2}) was used as working electrode, graphite rod as counter electrode and Ag/AgCl as reference electrode. All potentials were referenced to reversible hydrogen electrode (RHE) according to the equation: E (V vs. RHE) = E (V vs. Ag/AgCl) + 0.198 V + 0.059 × pH. The NO_2RR measurements were carried out in 0.5 M Na_2SO_4 + 0.1 M $NaNO_2$ electrolyte using an H-type two-compartment electrochemical cell separated by a Nafion 211 membrane. The Nafion membranes were pretreated by boiling in 5% H_2O_2 solution for 1 h, in 0.5 M H_2SO_4 for 1 h and in deionized water for 1 h. Prior to NO_2RR electrolysis, the cathodic compartment was purged with Ar for 30 min. After each chronoamperometry test for 1 h, the produced NH_3 and other possible by-products (NO_2^- and N_2H_4) were analyzed by various colorimetric methods using UV-vis absorbance spectrophotometer (MAPADA P5), while the gas products were analyzed by gas chromatography (Shimadzu GC2010).

Determination of NH_3

The NH_3 concentration was determined by the indophenol blue method[1]. Firstly, the diluted sample solution (2 mL) was sequentially added to 2 mL of 1 M NaOH coloring solution containing 5% salicylic acid and 5% sodium citrate, 1 mL oxidizing solution of NaClO (4.5%) and 0.2 mL catalyst solution of $C_5FeN_6Na_2O$ (1 wt%). After standing in the dark for 2 h at room temperature, the absorbance values of NH_3 concentrations were expressed as absorption peaks at 655 nm and the concentration-absorbance curves were calibrated with different concentrations of standard NH_4Cl solutions.

NH_3 yield rate was calculated by the following equation:

$$\text{NH}_3 \text{ yield rate } (\mu\text{mol h}^{-1}\text{ cm}^{-2}) = \frac{c_{\text{NH}_3} \times V}{t \times A} \quad (1)$$

NH_3-Faradaic efficiency (FE_{NH3}) was calculated by the following equation:

$$\text{FE}_{\text{NH3}}(\%) = \frac{6 \times F \times c_{\text{NH}_3} \times V}{M \times Q} \times 100\% \quad (2)$$

where c_{NH3} is the measured NH_3 concentration, V (mL) is the volume of the electrolyte, t (h) is the reduction time and A (cm^{-2}) is the mass loading of the catalyst on CC (1 × 1 cm^2). M molar mass of NH_3, F (96500 C mol^{-1}) is the Faraday constant, and Q (C) is the quantity of applied electricity.

Determination of N_2H_4

The concentration of N_2H_4 was determined by Watt and Chrisp method[2]. Coloring solution was prepared by mixing 300 mL C_2H_5OH, 5.99 g $C_9H_{11}NO$ and 30 mL HCl. Then, 5 mL color solution was added into 5 mL electrolyte. After the incubation for 20 min at room temperature, the mixed solution was subjected to UV-vis measurement using the absorbance at 455 nm wavelength. The concentration-absorbance curves were calibrated by the standard N_2H_4 solution with a series of concentrations.

Nuclear magnetic resonance (NMR) measurement

^1H nuclear magnetic resonance (NMR) measurement was performed to confirm the source of generated NH_3. After chronoamperometry tests in Ar-saturated 0.1 M NaOH with 0.1 M $^{15}NO_2^-$ at -0.6 V for 1 h, 4 mL of electrolyte was removed from the electrochemical reaction vessel, which was concentrated to 1 mL and further acidized to pH 2. The obtained electrolyte was mixed with 0.1 mL of deuterium oxide (D_2O) containing 100 ppm of dimethyl sulphoxide (DMSO) and 70 μL of D_2O for NMR spectroscopy measurement (500 MHz Bruker superconducting-magnet NMR spectrometer.

Calculation details

DFT calculations were carried out using a Cambridge sequential total energy package (CASTEP). The generalized gradient approximation (GGA) with the Perdew–Burke–Ernzerhof (PBE) exchange-correlation function was utilized in the

calculations. The DFT-D correction method was considered for van der Waals forces. During the geometry optimization, the convergence tolerance was set to be 1.0×10^{-5} eV for energy and 0.02 eV $Å^{-1}$ for force. The 2×2×1 Monkhorst-Pack mesh was used in Brillouin zone sampling. The electron wave functions were expanded using plane waves with a cutoff energy of 400 eV. Mo_2C (001) was modeled by a 5 × 5 supercell, and a vacuum region of 15 Å was used to separate adjacent slabs.[3]

The Gibbs free energy (ΔG, 298 K) of reaction steps is calculated by[4]:

$$\Delta G=\Delta E+\Delta ZPE-T\Delta S \quad (3)$$

where ΔE is the adsorption energy, ΔZPE is the zero-point energy difference and $T\Delta S$ is the entropy difference between the gas phase and adsorbed state. The entropies of free gases were acquired from the NIST database.

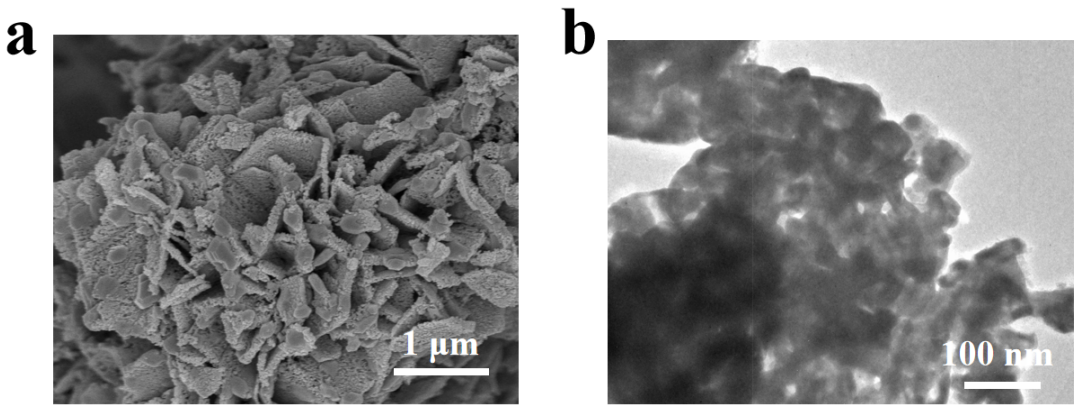

Fig. S1. Characterizations of pristine Mo_2C: (a) SEM image, (b) TEM image.

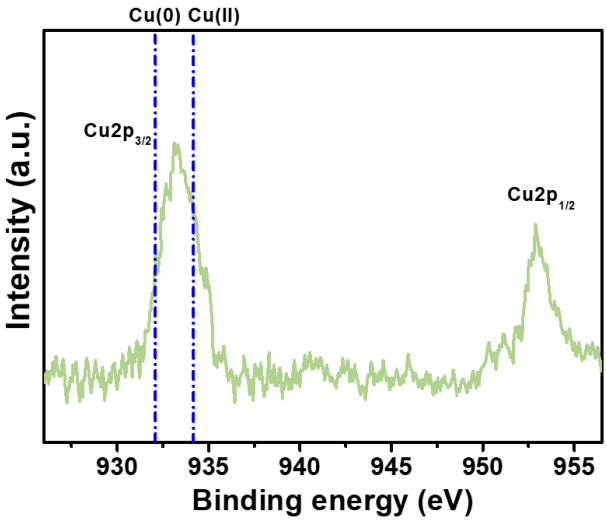

Fig. S2. XPS Cu 2p spectra of Cu_1/Mo_2C.

The XPS Cu 2p spectrum of Cu_1/Mo_2C indicates that the valence state of Cu is between +0 and +2, consistent with the XAS result.

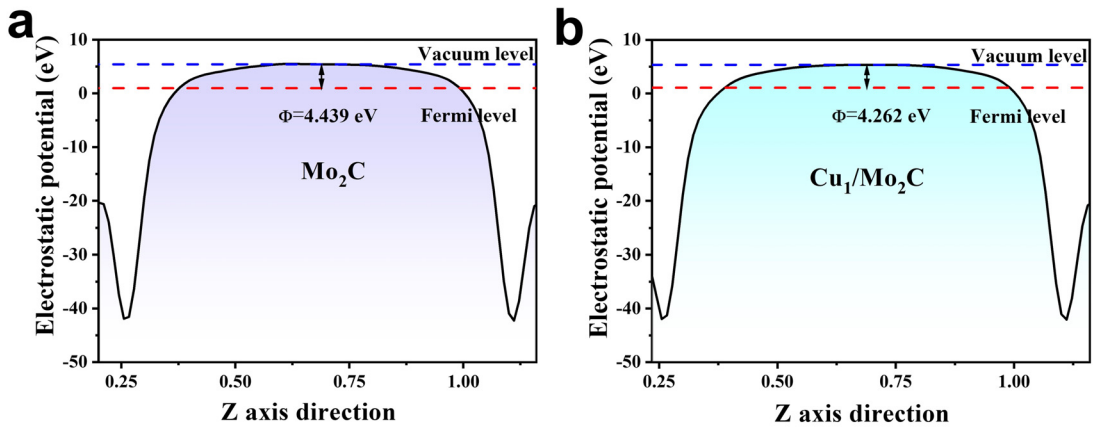

Fig. S3. Calculated work functions of Mo_2C and Cu_1/Mo_2C.

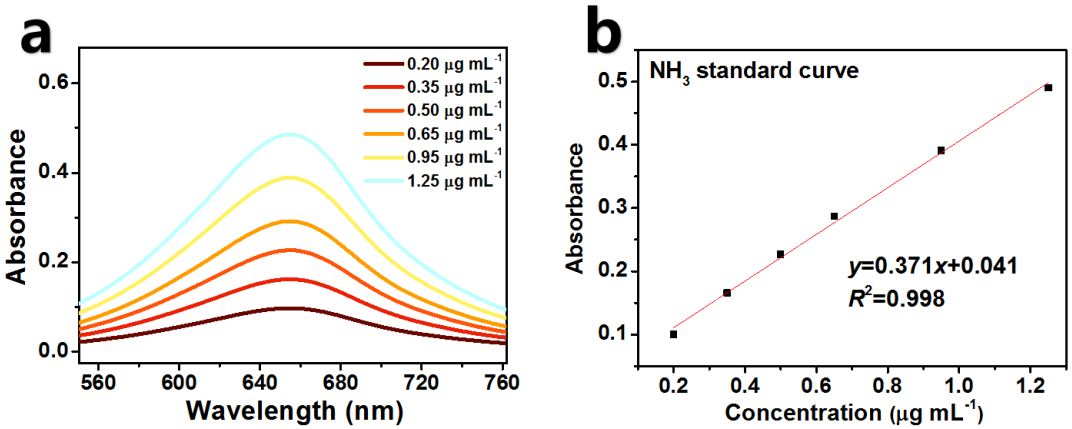

Fig. S4. (a) UV-vis absorption spectra of NH_4^+ assays after incubated for 2 h at ambient conditions. (b) Calibration curve used for the calculation of NH_3 concentrations.

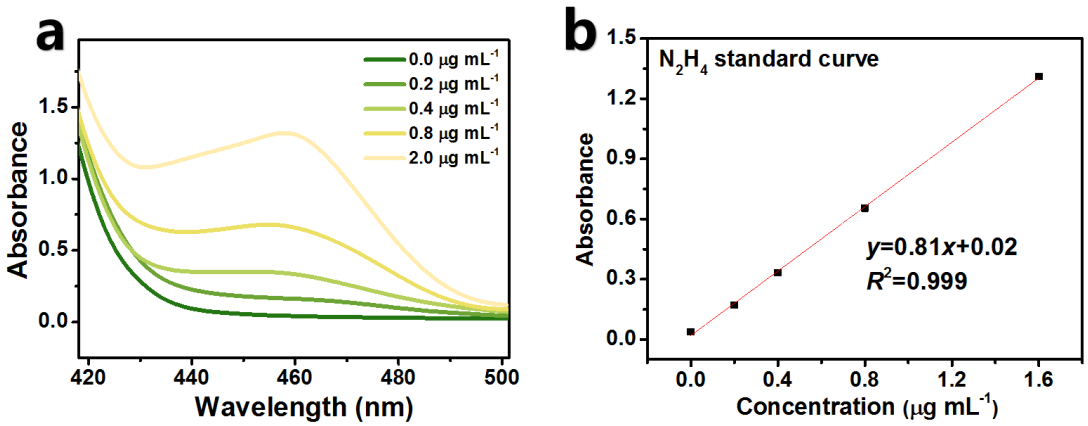

Fig. S5. (a) UV-vis absorption spectra of N_2H_4 assays after incubated for 20 min at ambient conditions. (b) Calibration curve used for calculation of N_2H_4 concentrations.

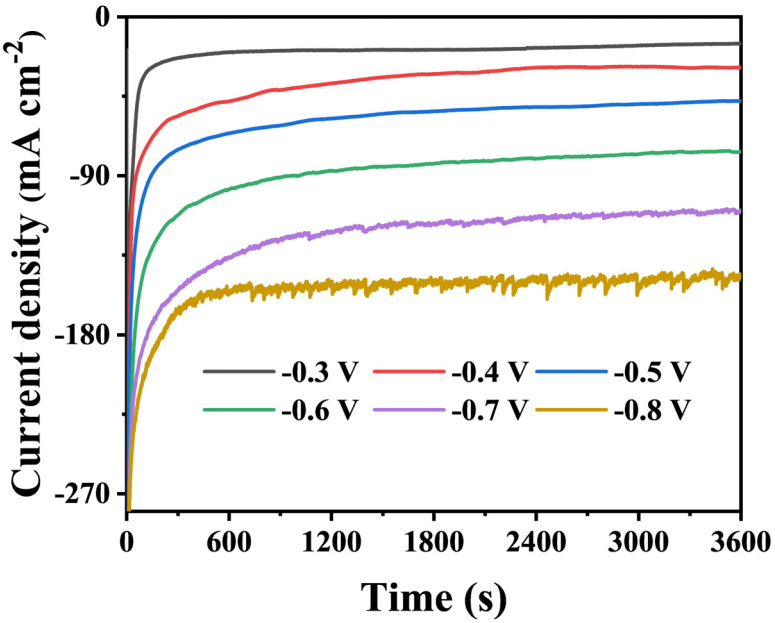

Fig. S6. Chronoamperometry curves of Cu_1/Mo_2C after 1 h electrolysis at various potentials.

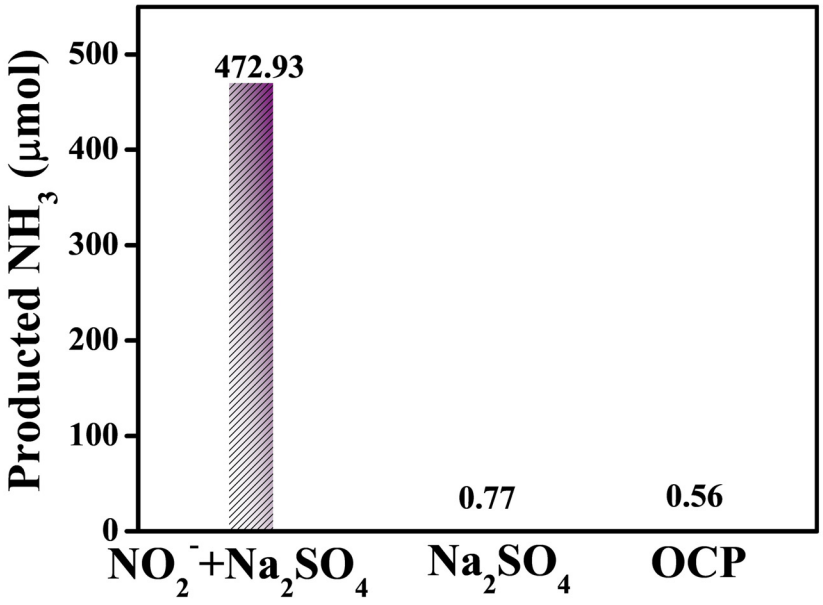

Fig. S7. Amounts of produced NH_3 on Cu_1/Mo_2C under different conditions: (1) electrolysis in NO_2^--containing solution at −0.6 V, (2) electrolysis in NO_2^--free solution at −0.6 V; (3) electrolysis in NO_2^--containing solution at open−circuit potential (OCP).

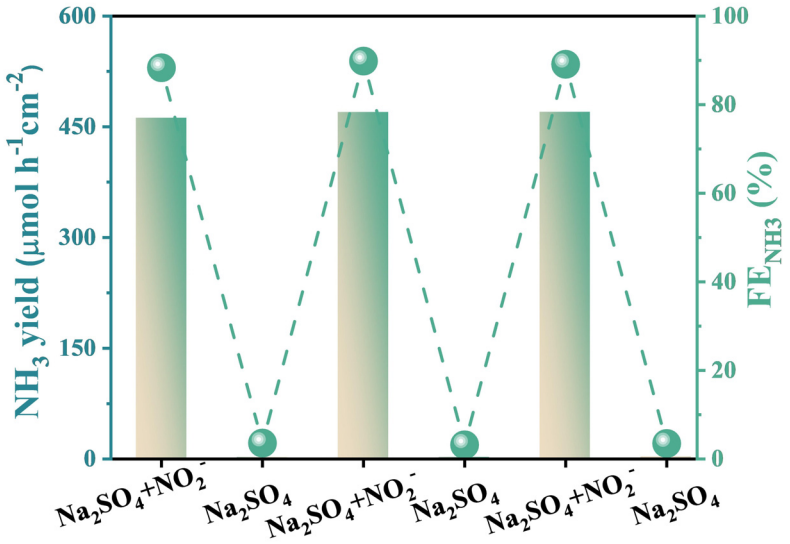

Fig. S8. NH_3 yield rates and FE_{NH3} during alternating cycle tests in 0.5 M Na_2SO_4 solution with and without NO_2^- at −0.6 V.

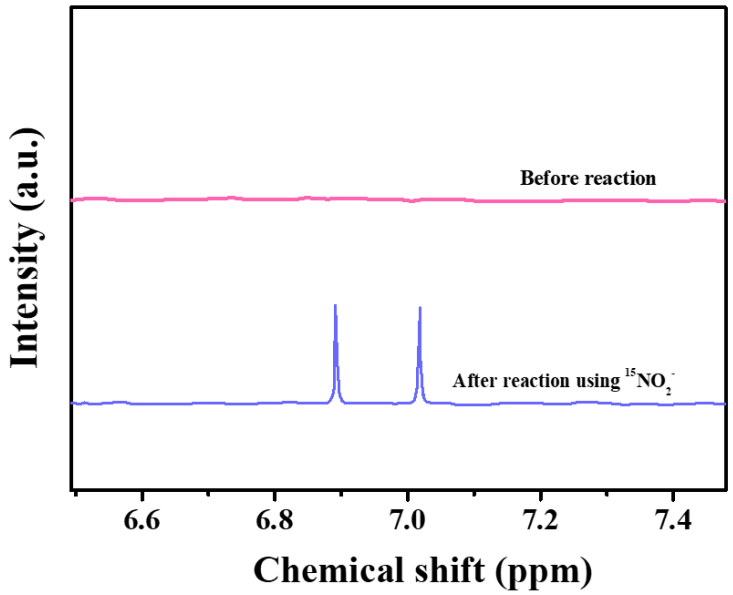

Fig. S9. ^{1}H NMR spectra of the electrolyte after electrolysis on Cu_1/Mo_2C at −0.6 V using $^{15}NO_2^-$ as feeding agents.

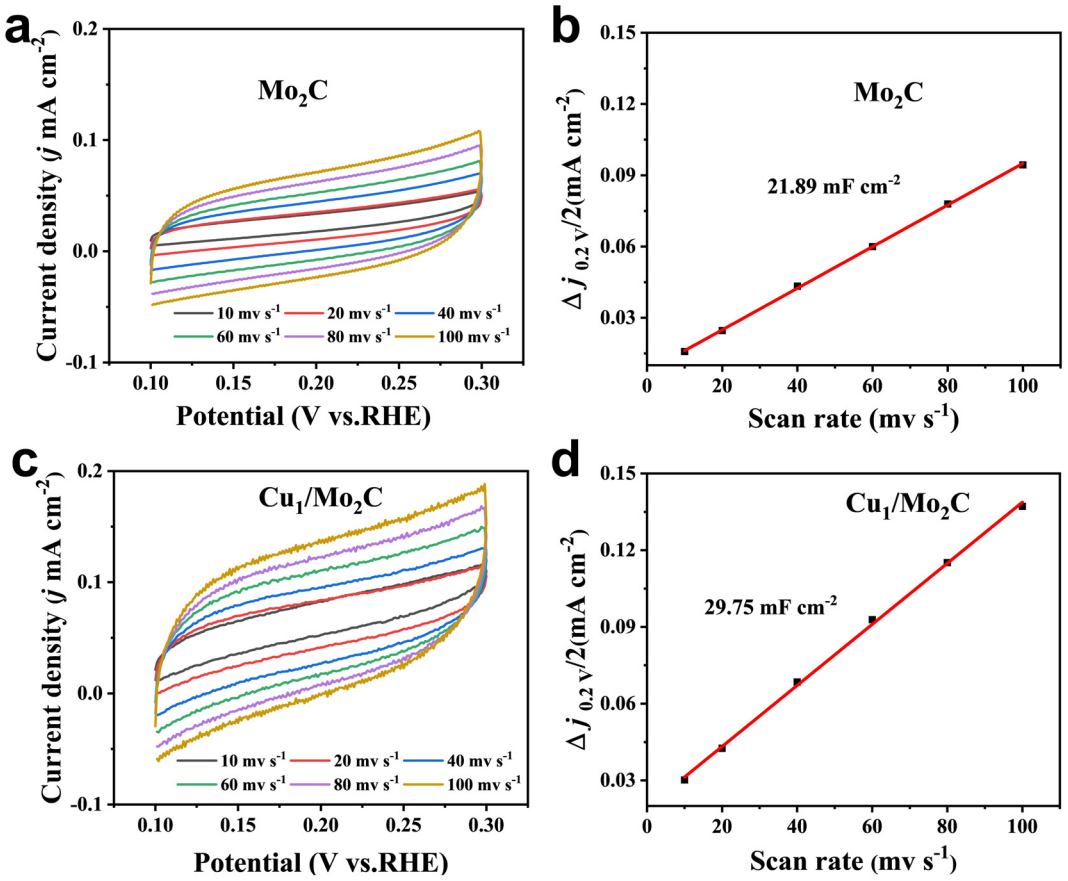

Fig. S10. Electrochemical double-layer capacitance (C_{dl}) measurements at different scanning rates of 10~100 mV s^{-1} for (a, b) Mo_2C and (c, d) Cu_1/Mo_2C.

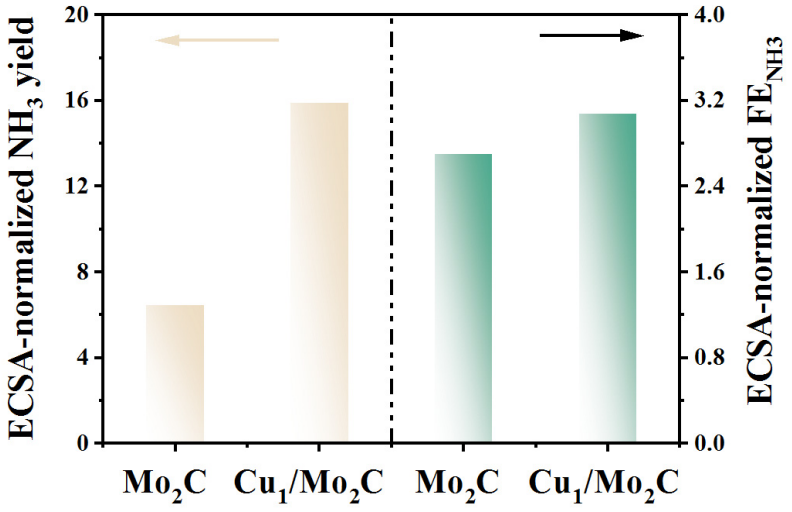

Fig. S11. Comparison of the ECSA-normalized NH_3 yield rates and FE_{NH3} between Mo_2C and Cu_1/Mo_2C at -0.6 V.

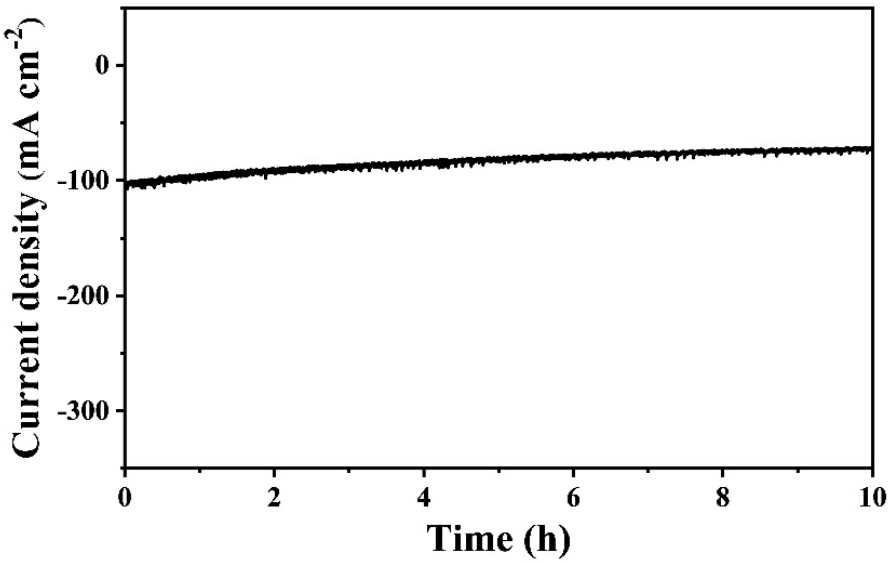

Fig. S12. Long-term durability test of Cu_1/Mo_2C during 10 h electrolysis at -0.6 V.

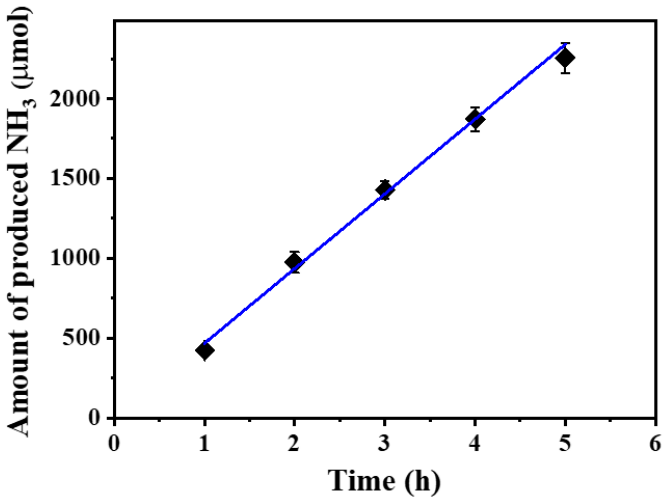

Fig. S13. Amount of produced NH_3 after NO_2RR electrolysis at various times (1-6 h) on Cu_1/Mo_2C at -0.6 V.

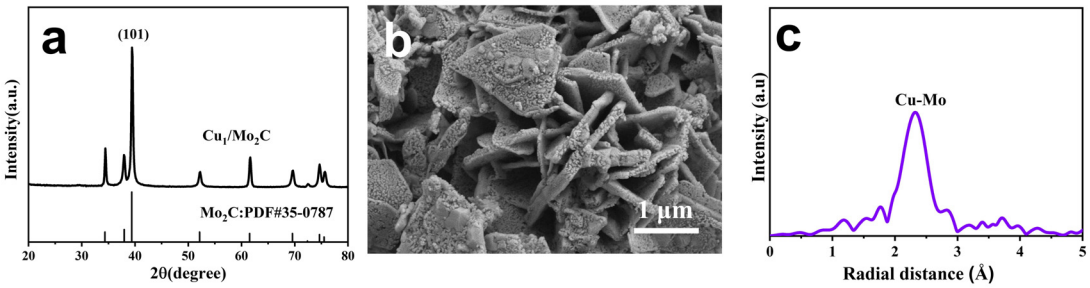

Fig. S14 (a) XRD pattern, (b) SEM image and (c) Cu K-edge EXAFS spectrum of Cu_1/Mo_2C after NO_2RR test.

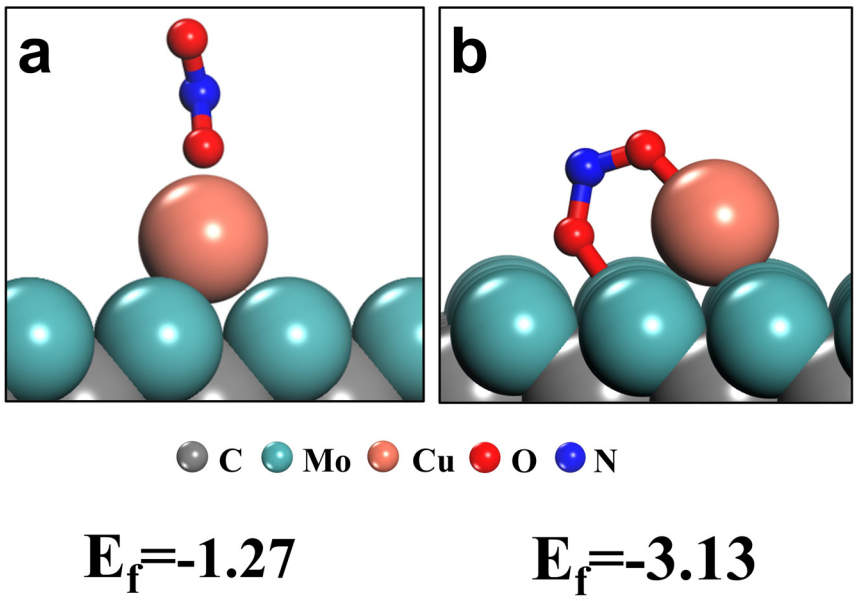

Fig. S15.Optimized structures of NO_2 adsorption models on (a) Cu alone and (b) both Cu and its adjacent Mo atoms.

It is noted that we have examined the optimized adsorption models of $*NO_2$ on Cu_1/Mo_2C, and it is shown in Fig. S15 that $*NO_2$ absorbed on both Cu atom and its adjacent Mo atoms has the lower adsorption energy compared to $*NO_2$ on Cu atom alone, indicating that Cu-Mo serves as the dual active centers to absorb and activate the $*NO_2$.

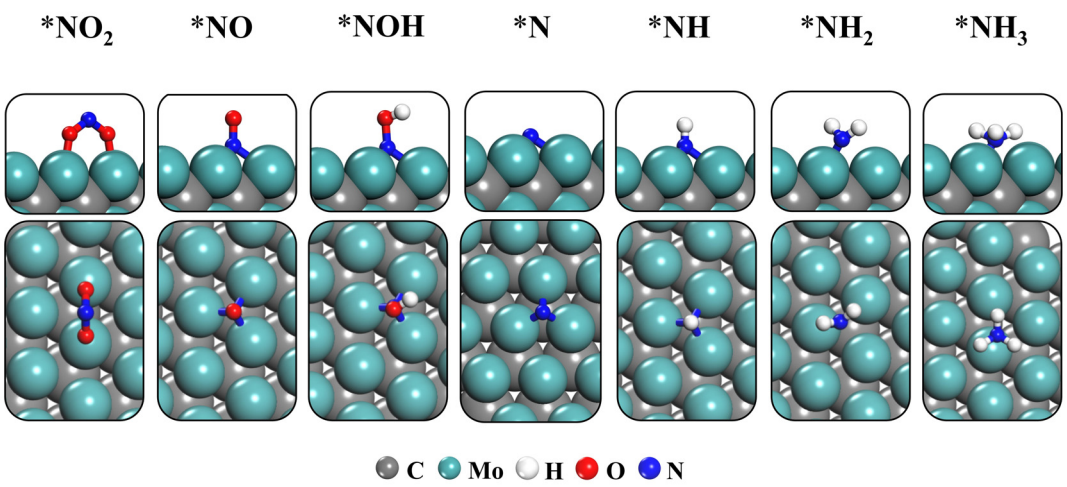

Fig. S16. Optimized structures of NO_2RR intermediates on bare Mo_2C.

Table S1. Cu K-edge EXAFS fitting results of Cu_1/Mo_2C

Sample	Shell	CN	R (Å)	$\sigma^2(10^{-3}$ Å)	ΔE_0 (eV)	R factor
Cu_1/Mo_2C	Cu-Mo	2.8	2.76	6.1	-3.7	0.007

CN is the coordination number, R is interatomic distance, σ^2 is Debye-Waller factor, ΔE_0 is edge-energy shift, R factor is used to value the goodness of the fitting.

Table S2. Comparison of optimum NH_3 yield and Faradic efficiency (FE) for recently reported state-of-the-art NO_2RR electrocatalysts at ambient conditions

Catalysts	Electrolytes	*NH_3 yield ($\mu mol\ h^{-1}\ cm^{-2}$)*	*FE_{NH3}/%*	Potential (V vs RHE)	*Ref.*
P-TiO_2/TP	0.1 M Na_2SO_4 (0.1 M NO_2^-)	560.8	90.6	-0.6 V	[5]
CoP NA/TM	0.1 M PBS (500 ppm NO_2^-)	132.7±3.0	90.0±2.3	-0.2 V	[6]
ITO@TiO_2/TP	0.5 M $LiClO_4$(0.1 M NO_2^-)	411.3	82.6	-0.5 V	[7]
Pd/CuO NOs	0.1 M K_2SO_4 (0.01 M NO_2^-)	53.3	91.8	-1.5 V	[8]
Ni_2P/NF	0.1 M PBS (200 ppm NO_2^-)	158.1 ± 5.4	90.2±3.0	-0.3 V	[9]
CF@Cu_2O	0.1 M PBS (0.1 M NO_2^-)	441.8	94.2	-0.6 V	[10]
MoS_2 NSs	0.5 M Na_2SO_4 (0.1 M NO_2^-)	528.8	93.52	-0.5 V	[11]
Ni-TiO_2/TP	0.1 M NaOH (0.1 M NO_2^-)	380.27	94.89	-0.5 V	[12]
NiS_2@TiO_2/TM	0.1 M NaOH (0.1 M NO_2^-)	485.4	92.1	-0.5 V	[13]
MoO_2/MP-12	0.5 M Na_2SO_4 (0.1 M NO_2^-)	510.5	94.5±0.2	-0.8 V	[14]
Cu_3P NA/CF	0.1 M PBS (0.1 M NO_2^-)	95.7±2.1	91.2±2.5	-0.5 V	[15]
CoB@TiO_2/TP	0.1 M Na_2SO_4 (400 ppm NO_2^-)	233.1	95.2	-0.7 V	[16]
Ag@NiO/CC	0.1 M NaOH (0.1 M NO_2^-)	235.4	97.7	-0.4 V	[17]
Cu_1/Mo_2C	**0.5 M NaOH (0.1 M NO_2^-)**	**472.9**	**91.5**	**-0.6 V**	**This work**

Supplementary references

[1]. D. Zhu, L. Zhang, R. E. Ruther and R. J. Hamers, *Nat. Mater.*, 2013, **12**, 836-841.

[2]. G. W. Watt and J. D. Chrisp, *Anal. Chem.*, 1952, **24**, 2006-2008.

[3]. S.-H. Joo, J. W. Bae, W.-Y. Park, Y. Shimada, T. Wada, H. S. Kim, A. Takeuchi, T. J. Konno, H. Kato and I. V. Okulov, *Adv. Mater.*, 2020, **32**, 1906160.

[4]. A. A. Peterson, F. Abild-Pedersen, F. Studt, J. Rossmeisl and J. K. Nørskov, *Energy Environ. Sci.*, 2010, **3**, 1311-1315.

[5]. L. Ouyang, X. He, S. Sun, Y. Luo, D. Zheng, J. Chen, Y. Li, Y. Lin, Q. Liu and A. M. Asiri, *J. Mater. Chem. A*, 2022, **10**, 23494-23498.

[6]. G. Wen, J. Liang, Q. Liu, T. Li, X. An, F. Zhang, A. A. Alshehri, K. A. Alzahrani, Y. Luo, Q. Kong and X. Sun, *Nano Res.*, 2022, **15**, 972-977.

[7]. S. Li, J. Liang, P. Wei, Q. Liu, L. Xie, Y. Luo and X. Sun, *EScience*, 2022, **2**, 382-388.

[8]. S. Liu, L. Cui, S. Yin, H. Ren, Z. Wang, Y. Xu, X. Li, L. Wang and H. Wang, *Appl. Catal. B*, 2022, **319**, 121876.

[9]. G. Wen, J. Liang, L. Zhang, T. Li, Q. Liu, X. An, X. Shi, Y. Liu, S. Gao, A. M. Asiri, Y. Luo, Q. Kong and X. Sun, *J. Colloid Interf. Sci.*, 2022, **606**, 1055-1063.

[10]. Q. Chen, X. An, Q. Liu, X. Wu, L. Xie, J. Zhang, W. Yao, M. S. Hamdy, Q. Kong and X. Sun, *Chem. Commun.*, 2022, **58**, 517-520.

[11]. L. Yi, P. Shao, H. Li, M. Zhang, X. Peng, K. Chen, X. Liu and Z. Wen, *J. Power Sources*, 2023, **559**, 232668.

[12]. Z. Cai, C. Ma, D. Zhao, X. Fan, R. Li, L. Zhang, J. Li, X. He, Y. Luo, D. Zheng, Y. Wang, B. Ying, S. Sun, J. Xu, Q. Lu and X. Sun, *Mater. Today Energy*, 2023, **31**, 101220.

[13]. X. He, L. Hu, L. Xie, Z. Li, J. Chen, X. Li, J. Li, L. Zhang, X. Fang, D. Zheng, S. Sun, J. Zhang, A. Ali Alshehri, Y. Luo, Q. Liu, Y. Wang and X. Sun, *J. Colloid Interf. Sci.*, 2023, **634**, 86-92.

[14]. G. Wang, Q. Chen, X. An, Q. Liu, L. Xie, J. Zhang, W. Yao, X. Liu, S. Sun, X. Sun and Q. Kong, *Colloid. Surface. A*, 2023, **657**, 130549.

[15]. J. Liang, B. Deng, Q. Liu, G. Wen, Q. Liu, T. Li, Y. Luo, A. A. Alshehri, K. A. Alzahrani and D. Ma, *Green Chem.*, 2021, **23**, 5487-5493.

[16]. L. Hu, D. Zhao, C. Liu, Y. Liang, D. Zheng, S. Sun, Q. Li, Q. Liu, Y. Luo, Y. Liao, L. Xie and X. Sun, *Inorg. Chem. Front.*, 2022, **9**, 6075-6079.

[17]. Q. Liu, G. Wen, D. Zhao, L. Xie, S. Sun, L. Zhang, Y. Luo, A. A. Alshehri, M. S. Hamdy, Q. Kong and X. Sun, *J. Colloid Interf. Sci.*, 2022, **623**, 513-519.